Psychological Medicine, 2001, **31**, 1437–1446. © 2001 Cambridge University Press
DOI: 10.1017/S0033291701004561 Printed in the United Kingdom

Widespread anatomical abnormalities of grey and white matter structure in tuberous sclerosis

K. RIDLER,[1] E. T. BULLMORE, P. J. DE VRIES, J. SUCKLING, G. J. BARKER, S. J. P. MEARA, S. C. R. WILLIAMS AND P. F. BOLTON

From the Brain Mapping Unit and Developmental Psychiatry Section, Department of Psychiatry, University of Cambridge; and Clinical Age Research Unit, Department of Health Care of the Elderly, Brain Image Analysis Unit, Department of Biostatistics & Computing and Department of Neurology, Institute of Psychiatry, King's College London and University Department of Clinical Neurology, Institute of Neurology, Queen Square, London

ABSTRACT

Background. Neuroimaging studies of tuberous sclerosis complex (TSC) have previously focused mainly on tubers or subependymal nodules. Subtle pathological changes in the structure of the brain have not been studied in detail. Computationally intensive techniques for reliable morphometry of brain structure are useful in disorders like TSC, where there is little prior data to guide selection of regions of interest.

Methods. Dual-echo, fast spin-echo MRI data were acquired from 10 TSC patients of normal intelligence and eight age-matched controls. Between-group differences in grey matter, white matter and cerebrospinal fluid were estimated at each intracerebral voxel after registration of these images in standard space; a permutation test based on spatial statistics was used for inference. CSF-attenuated FLAIR images were acquired for neuroradiological rating of tuber number.

Results. Significant deficits were found in patients, relative to comparison subjects, of grey matter volume bilaterally in the medial temporal lobes, posterior cingulate gyrus, thalamus and basal ganglia, and unilaterally in right fronto-parietal cortex (patients −20%). We also found significant and approximately symmetrical deficits of central white matter involving the longitudinal fasciculi and other major intrahemispheric tracts (patients −21%); and a bilateral cerebellar region of relative white matter excess (patients +28%). Within the patient group, grey matter volume in limbic and subcortical regions of deficit was negatively correlated with tuber count.

Conclusions. Neuropathological changes associated with TSC may be more extensive than hitherto suspected, involving radiologically normal parenchymal structures as well as tubers, although these two aspects of the disorder may be correlated.

INTRODUCTION

Tuberous sclerosis complex (TSC) is a multisystem genetic disorder associated with a range of physical, behavioural and cognitive manifestations. The prevalence of TSC is approximately one in 10000 live births (Osborne *et al.* 1991); it has an autosomal dominant pattern of inheritance with a spontaneous mutation rate up to 70% and a penetrance of almost 100%. Two genes associated with TSC have been cloned: TSC1 on chromosome 9q34 (van Slegtenhorst *et al.* 1997) encodes the protein hamartin; and TSC2 on chromosome 16p13.3 (Nellist *et al.* 1993) encodes the protein tuberin. Both tuberin and hamartin have been shown to act as tumour suppressors, most likely through GTPase activating protein (GAP) domains (Soucek *et al.* 1997).

Although the genetic basis for tuberous

[1] Address for correspondence: Ms Khanum Ridler, Brain Mapping Unit, Department of Psychiatry, University of Cambridge, Box 189, Addenbrooke's Hospital, Cambridge CB2 2QQ.

sclerosis is well-delineated, the clinical phenotype is protean. This marked variation in clinical expression of the disorder is best understood using Knudson's 'two hit model' of pathogenesis (Knudson, 1971). According to this model, affected individuals with TSC either inherit or develop as a spontaneous mutation one abnormal copy of the TSC gene. Phenotypic manifestations then occur only after a 'second hit', which inactivates the second copy of the TSC gene and the protein it encodes. This variability of expression leads to a wide range of presentations, with cerebral manifestations of the disorder generally causing the greatest clinical problems. The cognitive and behavioural consequences of TSC may vary with age and are not inevitably severe: up to one-third of patients may have normal intelligence (Harrison & Bolton, 1997). However, frequent psychopathological outcomes in childhood include autism, hyperactivity, mental handicap and intractable epilepsy; and in adulthood there are also reports of hallucinations, delusions, high levels of anxiety and obsessive behaviours (Harrison & Bolton, 1997; de Vries *et al*. 2001*a*).

Pathologically, tuberous scelorosis is a phakomatosis characterized by foci of abnormal tissue development (dysplasia) and by the appearance of developmental tumours (hamartomata) in brain, eyes, kidneys, heart and skin. Well-recognized abnormalities of cerebral structure in TSC include: (*i*) dysplastic grey matter formations such as clusters of neurons heterotopically located outside cortex and subcortical nuclei; (*ii*) tubers (or hamartomata) typically located in cortex and affecting the white matter immediately subjacent to cortex and (*iii*) abnormalities arising immediately beneath the ependymal lining of the ventricles called subependymal nodules (SENs) which occur in 95% of patients (Scheithauer & Reagan, 1999). SENs may undergo neoplastic change to subependymal giant cell astrocytomas (SEGA), in approximately 8% of patients (Shepherd *et al*. 1991). Tuber size, number and location vary markedly between subjects. However, tubers are predominantly distributed in the frontal, temporal and parietal lobes (Braffman *et al*. 1992). Subcortical white matter close to tubers usually shows hyperintense changes on fast spin-echo (FSE) MR-images, most likely due to gliosis and hypomyelination in this tissue (Marti-Bonmati *et al*. 2000).

Besides these distinctly abnormal and circumscribed pathological features of the brain in TSC, there is also some evidence for more subtle abnormalities of brain parenchymal structure. For example, though whole brain weight is usually normal, there have been reports of non-obstructive hydrocephalus, cerebellar atrophy (Marti-Bonmati *et al*. 2000), and reduced volume of the hippocampal formation (Scheithauer & Reagan, 1999). It is unclear whether these observations can be attributed to the neurotoxic effects of chronic epilepsy and/or its treatment (Scheithauer & Reagan, 1999) or whether they represent a primary aspect of the disorder. It seems likely that some abnormalities of cortical and cerebellar structure may be associated with the local presence of tubers (Marti-Bonmati *et al*. 2000); although it remains unknown whether tuber formation causes parenchymal damage, or vice versa, or whether these are correlated consequences of the same underlying genetic lesion.

Neuroimaging studies have been able to identify tubers and subependymal nodules *in vivo* and to correlate these abnormalities with clinical and behavioural aspects of the disorder (Jambaque *et al*. 1991; Shepherd *et al*. 1995; Bolton & Griffiths, 1997; Harrison *et al*. 1999). There have been very few previous imaging studies of other possible changes in brain structure in apparently normal tissue in patients with TSC. Studies so far have focused on structural changes due to an identified visible abnormality, such as cortical gyral expansion (Braffman *et al*. 1992) or focal cerebellar atrophy (Marti-Bonmati *et al*. 2000), associated with the local presence of tubers. The study of possible parenchymal deficits in regions without radiological evidence for tubers has been limited by the universal adoption hitherto of a region-of-interest (ROI) approach to morphometry. This entails prior definition of a number of brain regions that are considered likely to be of special relevance to the disorder under investigation. However, in tuberous sclerosis complex there are insufficient prior data to inform this definition and computational morphometric techniques, which allow comprehensive and reliable assessment of brain structure without

prior constraints on the regions to be examined, may be more appropriate and informative.

METHOD

Subjects

Ten patients with tuberous sclerosis (four male, six female), and eight normal comparison subjects (five male, three female) matched for mean age and intelligence with the patient group were studied; see Table 1 for details of the sample. All patients satisfied standard operationalized diagnostic criteria for TSC (Roach *et al*. 1998). All participants were of normal intelligence as assessed using the National Adult Reading Test (NART); each participant's error score on the NART was used to derive an estimated Wechsler Adult Intelligence Scale-Revised (WAIS-R) Full-Scale IQ, using the formula of Nelson & Willison (1991). Five of the ten TSC patients had lifetime experience of at least one epileptic seizure; of those five patients, only two patients were receiving anti-convulsant medication, and only one patient experienced any seizures in the year prior to scanning. None of the participants had a history of cognitive deficits or psychiatric illness including autism.

Ethical approval for the study was obtained from the Ethics Committee (Research) of the Bethlem Royal and Maudsley NHS Trust and the Cambridge Local Research Ethics Committee. Written informed consent was obtained from all patients prior to the study.

Structural MR image acquisition

All patients were scanned using a GE Signa 1.5 Tesla system (General Electric, Milwaukee, WI, USA) at the Maudsley Hospital, London. A preliminary localizing scan in the sagittal plane was used to identify anterior and posterior commissures and to prescribe acquisition of a dual-echo FSE dataset in a near-axial plane parallel to the intercommissural line. Fifty contiguous, interleaved, 3 mm thick proton density (PD-) and T2-weighted images were acquired providing whole brain coverage. Repetition time (TR) was 4000 ms; echo times (TE) were 20 ms and 85 ms with an eight-echo train length. The matrix size was 256×192 and the field of view was 22 cm, giving an in-plane resolution of 0·859 mm. The total acquisition time was 10 min and 12 s. Fast (cerebrospinal) fluid-attenuated inversion recovery (Fast-FLAIR) images were also acquired from the 10 TSC patients in the same (near-axial) orientation as the FSE images. For the Fast-FLAIR data, TR was 10 500 ms, TE was 144 ms with a 16-echo train length, there were two excitations, inversion time (TI) was 2190 ms, matrix size was 256×192, slice thickness was 3 mm, and the total acquisition time was 8 min and 24 s.

Structural MRI data analysis

The methods used for segmentation and registration of each FSE dataset have been described in detail elsewhere (Brammer *et al*. 1997; Suckling *et al*. 1999*a*). Briefly, voxels representing extra-cerebral tissue were automatically identified and set to zero using a linear scale-space set of features obtained from derivatives of the Gaussian kernel (Suckling *et al*. 1999*b*). Manual editing of the segmented images was necessary only to remove the brainstem (from below a line parallel to the base of the cerebellum) from the diencephalon and cerebral hemispheres. The probability of each intracerebral voxel belonging to each of four possible tissue classes (grey matter, white matter, CSF or dura/vasculature) was then estimated by a modified fuzzy clustering algorithm (Suckling *et al*. 1999*a*). Based on prior results, we assumed that the resulting probabilities of tissue class membership could be equated with the proportional volumes of each tissue class in the often heterogeneous volume of tissue repre-

Table 1. *Sample demographics*

	TSC	Non-TSC	*t*	*P*
Sample size (*N*)	10	8		
Sex ratio (M:F)	4:6	5:3		
Average age (S.D.)	41·5 (14·6)	40·0 (13·0)	−0·0299	0·822
Average IQ measured by the NART (S.D.)	109·9 (10·3)	111·3 (13·8)	0·238	0·81

https://doi.org/10.1017/S0033291701004561 Published online by Cambridge University Press

sented by each voxel (Bullmore *et al*. 1995). For example if the probability of grey matter class membership was 0·8 for a given voxel then it was assumed that 80% of the tissue represented by that voxel was grey matter. Given the voxel dimensions in millimetres, it was straightforward to estimate the volume in millilitres of grey matter, or any other tissue class, at each voxel. Summing these voxel tissue class volumes over all intracerebral voxels yielded global tissue class volumes.

To allow estimation of between-group structural differences at each intra-cerebral voxel, the PD-weighted images from each FSE dataset were first co-registered with a template image in the standard stereotactic space of Talairach & Tournoux (1988) by a 12-parameter affine transformation implemented using the Fletcher-Davidon-Powell optimization algorithm (Press *et al*. 1992; Brammer *et al*. 1997). The template image was constructed by proportional rescaling of the distances between anatomical landmarks identified in PD–weighted images of five normal controls using AFNI software (Cox, 1995). The parameters of the affine transformation, which minimized mismatch between an individual PD-weighted image and the template image, were then applied in turn to each of that individual's tissue class probability maps to register them in standard space.

An analysis of covariance (ANCOVA) model was fitted at each voxel in standard space for which we had spatially overlapping data on all 18 participants. The model is written below with grey matter proportional volume as the dependent variable; formally identical models were fitted separately with white matter and CSF volumes as the dependent variable:

$$G_{kj} = \mu + \alpha_k \mathrm{Group}_{kj} + \beta \mathrm{Age}_{kj} + \delta \mathrm{Sex}_{kj} + \eta \mathrm{Global}_{kj} + \epsilon_{kj}. \quad (1)$$

Here G_{kj} denotes the proportional volume of grey matter estimated at a given voxel for the jth individual in the kth group; μ is the overall mean; $\mu + \alpha_k$ is the mean of the kth group; and ϵ_{kj} is random variation. The independent variables Group_{kj}, Age_{kj}, Sex_{kj} and Global_{kj} denote the diagnostic group (TSC patient or comparison subject), age, gender and global tissue volume (in this case, global grey matter volume) of the jth individual in the kth group.

Fitting this model at each intra-cerebral voxel of the observed data, with the proportional volumes for each tissue class taken in turn as the dependent variable, yields a set of three 'effect maps' of coefficient α divided by its standard error: i.e. $\alpha^* = \alpha/\mathrm{SE}(\alpha)$. To test the null hypothesis that $\alpha^* = 0$, we used a permutation test at the level of suprathreshold voxel clusters, as described in detail by Bullmore *et al*. (1999). In brief, the observed voxel statistic map of α^* was thresholded against the 2·5 and 97·5 percentiles of the permutation distribution of α^*, which had been ascertained by repeatedly (10 times) fitting the regression model at each voxel after random permutation of the vector coding group membership, and pooling the resulting estimates of α^* under the null hypothesis over all intracerebral voxels. Applying this probability threshold (two-tailed voxel-wise $P < 0{\cdot}05$) at each voxel of the observed maps generated a number of suprathreshold voxel clusters that were spatially contiguous in 3D. The sum of suprathreshold voxels in each such cluster was tested against a permutation distribution ascertained by applying the same probability threshold to each of the voxel statistic maps generated after random permutation of the vector coding group membership (Group). The rationale for this non-parametric mode of inference is that test statistics for image analysis which incorporate spatial neighbourhood information, such as 3D cluster size, are generally more powerful than other possible test statistics, such as α or α^*, which are informed only by data at a single voxel. Yet theoretical approximations to the null distributions of spatial statistics estimated in imaging data may be over-conservative or intractable (Bullmore *et al*. 1999; Ashburner & Friston, 2000).

Another advantage of hypothesis testing at cluster level is that the number of tests to be conducted, or search volume V, will generally be less by about two orders of magnitude than the number of tests that would be required at voxel level. This means that satisfactory type 1 error control can be attained with less risk of unacceptable type 2 error. Thus, in the analyses reported below, cluster-wise probability of type 1 error $P < 0{\cdot}001$ was chosen because at this size of test the expected number of false positive tests PV was less than one.

Neuroradiological analysis of FLAIR data

FLAIR and FSE data acquired from patients with TSC were visually inspected by three neuroradiologists who were blind to diagnosis. The total number of tuberous lesions present in each patient was agreed by consensus between three raters. These counts were correlated with the volume of grey matter in regions identified as structurally different between groups by prior computational morphometry. Spearman's non-parametric correlation coefficient ρ was used for this purpose because of non-normality of data and the small sample size.

RESULTS

Global tissue class volumes

Estimated volumes of whole brain and each of the three main tissue classes (grey matter, white matter and CSF) are shown in Table 2. There were no significant differences between groups on any of these measures.

Localized between-group differences in grey matter volume

Significant differences between TSC patients and comparison subjects in grey matter volume were identified bilaterally in the following brain regions: (*a*) medial temporal lobe and posterior cingulate gyrus, encompassing uncus, amygdala, hippocampus, parahippocampal gyrus and extending posteriorly and superiorly to posterior cingulate gyrus; and (*b*) subcortical structures, specifically the ventral basal ganglia (putamen, globus pallidus and caudate nuclei), hypothalamus, thalamus, claustrum and cerebellum; see Fig. 1. Over all these regions, grey matter volume was reduced by 18·6% in patients relative to comparison subjects (see Table 2); two-sample t test, $t = 5{\cdot}3$, df = 16, $P < 0{\cdot}0001$. There was also a significant between-group

Table 2. *Volumes (ml) of whole brain, grey matter, white matter and CSF as well as the volumes of grey and white 'deficit' and 'excess' regions identified by computational morphometry*

	Patients $N = 10$ Vol (S.D.)	95% CI of mean	Controls $N = 8$ Vol (S.D.)	95% CI of mean	t	P	95% CI of difference
Whole brain	1390·04 (69)	1337–1443	1392·66 (73)	1334–1436	0·077	0·940	−69·5 to 74·7
Grey matter	566·37 (63)	521–612	587·57 (40)	554–621	0·819	0·415	−33·7 to 76·1
White matter	572·85 (28)	553–593	550·98 (41)	516–586	−1·332	0·201	−56·7 to 12·9
CSF	182·90 (42)	153–213	187·58 (27)	165–210	0·270	0·790	−32·0 to 41·4
Total grey matter 'deficit'	16·50 (2)	15–18	20·64 (1)	19–22	5·699	0·00003	2·6 to 5·7
Total white matter 'deficit'	25·40 (2)	24–27	32·26 (2)	30–34	6·642	< 0·00001	4·7 to 9·0
White matter 'excess'	5·90 (1)	5–7	4·26 (2)	3–6	−2·756	0·014	−2·9 to −0·4

Table 3. *Regional differences in grey and white matter*

Cerebral region	Side	N	X	Y	Z
Grey matter					
Deficits					
Medial, temporal & posterior cingulate/subcortical	Bilateral	4471	1·6	−17	−1·7
Neocortical	Right	520	52·5	−5·9	31·5
White matter					
Deficits					
Anterior commissura, inferior longitudinal fasciculus, tapetum & superior longitudinal fasciculus	Right	1674	39·6	−20·2	5·8
Occipito-frontal fasciculus & cingulum	Right	1154	17·5	24·8	19·5
Occipito-frontal fasciculus, superior longitudinal fasciculus & cingulum	Left	1346	−23·2	9·1	25·8
Excesses					
Cerebellum	Bilateral	1048	6·0	−44·5	−16·4

The location of each cluster's centroid is given in Talairach co-ordinates (X, Y, Z; mm), N = number of voxels in each cluster. Cluster-wise probability threshold $P < 0{\cdot}001$.

https://doi.org/10.1017/S0033291701004561 Published online by Cambridge University Press

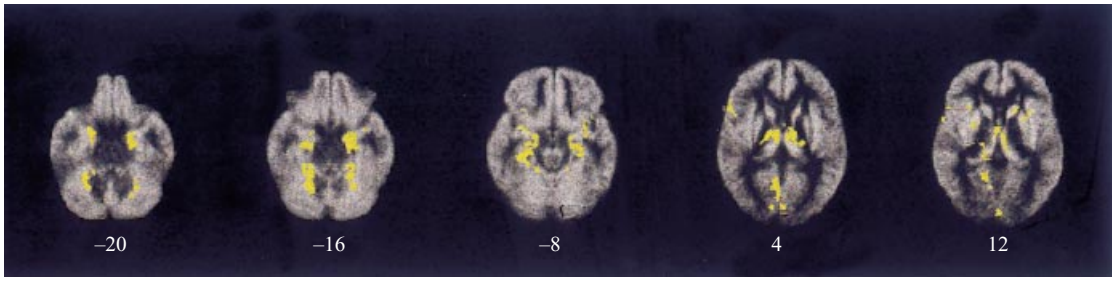

FIG. 1. Localized between-group differences in grey matter. Yellow regions show relative deficits in grey matter volume in the group of patients with tuberous sclerosis relative to normal comparison subjects. The cluster-wise probability of type 1 error $P < 0{\cdot}001$; the search volume V or number of clusters tested = 947; therefore the expected number of false positive tests over the whole map PV is less than one. The maps are orientated with the right side of the brain on the left side of each panel; the Z coordinate for each axial slice in the standard space of Talairach & Tournoux (1988) is given in millimetres.

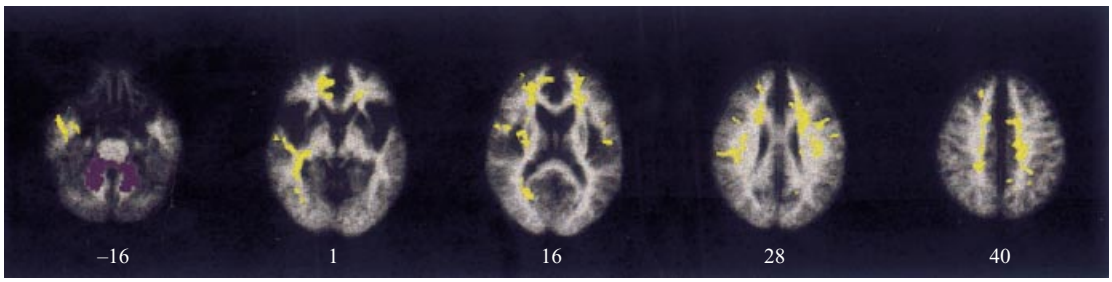

FIG. 2. Localized between-group differences in white matter. Yellow regions show relative deficits in white matter volume in the group of patients with tuberous sclerosis compared to normal comparison subjects; purple regions show relative excess in white matter volume in subjects. The cluster-wise probability of type 1 error $P < 0{\cdot}001$; the search volume V or number of clusters tested = 668; therefore the expected number of false positive tests over the whole map PV is less than one. The maps are orientated with the right side of the brain on the left side of each panel; the Z coordinate for each axial slice in the standard space of Talairach & Tournoux (1988) is given in millimetres.

difference in grey matter volume unilaterally in the right inferior frontal gyrus and right inferior parietal lobe; see Fig. 1. The total volume deficit in these regions was approximately 31% in patients (see Table 2); two-sample t test, $t = 5{\cdot}7$, df = 16, $P < 0{\cdot}0001$.

Localized between-group differences in white matter volume

Significant differences between TSC patients and comparison subjects in white matter volume were identified extensively and symmetrically throughout much of the central white matter, involving many of the major intrahemispheric tracts; see Fig. 2. More specifically, there were areas of deficit in the patients in the right inferior longitudinal fasciculi, extending to the right anterior commissure and tapetum; in the left and right cingulum; in the left and right occipito-frontal fasciculi; and in the right and left superior longitudinal fasciculi. Overall, white matter volume in the deficit regions was reduced by approximately 21% in subjects; two-sample t test, $t = 6{\cdot}64$, df = 16, $P < 0{\cdot}000006$ (see Table 2 cluster details). There was also a significant between-group difference in white matter volume bilaterally in the cerebellar medulla, but this was due to a relative excess of white matter volume in the subjects; see Fig. 2. Overall, white matter volume in the cerebellar region was 28% greater in subjects; two sample t test, $t = -2{\cdot}76$, df = 16, $P < 0{\cdot}014$.

Localized between-group differences in CSF volume

There were no significant, localized differences between TSC patients and comparison subjects in anatomical distribution of cerebrospinal fluid.

Correlation between tuber count and volume deficits

The total volume of grey matter in the neocortical, limbic and subcortical regions identified as deficient in patients by computational analysis

https://doi.org/10.1017/S0033291701004561 Published online by Cambridge University Press

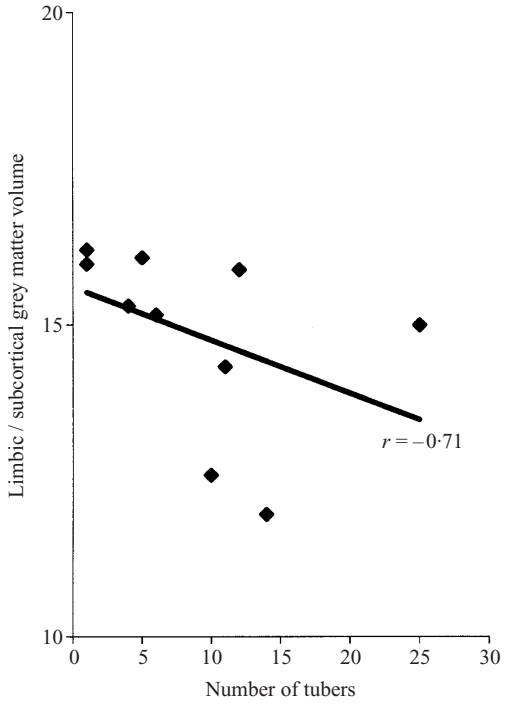

FIG. 3. The relationship between number of tubers (*X* axis) counted by neuro-radiological examination of FLAIR data and the volume (*Y* axis) of grey matter in limbic/subcortical regions of deficit identified by computational morphometric analysis of FSE data. Solid line indicates the fitted regression of grey matter volume on tuber count.

was negatively correlated with the number of tubers counted radiologically: $\rho = -0{\cdot}62$, df = 9, $P < 0{\cdot}056$. This correlation was slightly stronger when only limbic and subcortical regions of deficit were included in the analysis: $\rho = -0{\cdot}71$, df = 9, $P < 0{\cdot}021$; see Fig. 3. The association between tuber count and neocortical (right fronto-parietal) grey matter deficit was not significant: $\rho = -0{\cdot}47$, df = 9, $P < 0{\cdot}17$.

The total volume of white matter deficit regions was not significantly correlated with the number of tubers counted radiologically; $\rho = 0{\cdot}036$, df = 9, $P = 0{\cdot}920$. Neither was there a significant correlation between overall volumes of grey and white matter deficit: $\rho = 0{\cdot}103$, df = 9, $P = 0{\cdot}777$.

DISCUSSION

Comprehensive assessment of brain structure in magnetic resonance imaging data has shown extensive, bilateral, and approximately symmetrical deficits of grey and white matter in patients with tuberous sclerosis. The regions of grey matter deficit were almost exclusively in limbic structures of the medial temporal lobe and posterior cingulate gyrus, or in subcortical structures including thalamus, basal ganglia and cerebellum. Grey matter deficits in neocortex were limited to the right frontal and parietal cortex. There were deficits of white matter volume in the major intrahemispheric tracts bilaterally, and an excess of white matter bilaterally in the cerebellar medulla.

These findings are substantially novel. The existing neuropathological and neuroimaging literature has concentrated almost exclusively on hamartomata and focal dysplasias as the cerebral hallmarks of tuberous sclerosis. There have been no previous attempts to measure grey and white matter structure comprehensively throughout the brain and only a few prior studies of TSC have measured grey or white matter structure in association with a radiologically visible lesion in the brain. Intriguingly, some of our findings are compatible with the existing ROI literature. For example, we have found hippocampal volume deficits, which have previously been reported neuropathologically (Scheithauer & Reagan, 1999); and we have found an excess of white matter volume in cerebellum which echoes, albeit on a different scale of neural organization, previous reports of abnormal axonal formations in the cerebellum (Scheithauer & Reagan, 1999).

Before considering possible substantive interpretations of these results, we will address some of the methodological issues arising. First there is the question of sample size and between-group matching. The groups were both rather small (10 patients and eight controls) and not exactly matched for sex; see Table 1. However, we have tried to correct for possible confounding effects of a differential gender balance between the groups by including sex as a covariate in the analysis of covariance (ANCOVA) model, Equation 1, used to estimate between-group differences in anatomy. The smallness of the sample demands future replication of this study and its key results, and this work is in progress. Meanwhile, we note that the main statistical penalty of small sample size is increased type 2 (false negative) error; in other words, had this study

failed to find any anatomical differences between the groups, then small sample size might well have been regarded as a plausible culprit. Small sample size is a much less convincing explanation for the significant differences we have in fact observed, although the extent to which these findings might generalize to the population of patients with TSC currently remains open to question. A second methodological issue concerns the use of computational methods of morphometry. These methods have been fully described and validated elsewhere (Bullmore *et al.* 1999) but this kind of approach has not previously been used in tuberous sclerosis research and there may be some concern that the novelty of our findings is somehow an artefact of the morphometric methods. There are three main arguments against this interpretation. First, some of our findings, e.g. hippocampal grey matter deficit, have been demonstrated in prior studies; those of our findings that are not predicted by the existing literature concern regions that have not previously been considered of interest. Secondly, the statistical significance of deficits identified by a permutation test of spatial statistics has been corroborated by more conventional *t* tests of the difference between groups in grey and white matter volume in the regions of deficit. Thirdly, the severity of grey matter deficit defined by computational analysis of FSE data in limbic and subcortical structures was significantly, negatively correlated with the number of tubers counted by neuroradiological inspection of Fast-FLAIR data. This correlation between novel and more conventional methods of measuring pathological change in imaging studies of TSC may be pathologically interesting, but also provides some methodological support for the validity of the newer technique.

Turning now to possible substantive interpretations of these results, initially considering the deficits in grey matter volume, several aspects stand out. Systematic deficits in medial temporal lobe and basal ganglia structures were identified and these correlated with the number of tubers identified radiologically. Neuropathological studies have repeatedly demonstrated that one of the hallmarks of TSC are subependymal nodules (SENs) frequently found in the walls of the lateral ventricles especially around the head of the caudate and thalamus. SENs are thought to derive from cells in the ventricular zone that fail to migrate to the cortical plate during embryogenesis and then proliferate and differentiate abnormally. Therefore, grey matter deficits in the basal ganglia may well relate to the presence of abnormally differentiated cells within the basal ganglia and/or the failure of neuronal cells to migrate properly into these structures. The deficits in medial temporal lobe grey matter are easy to relate to the established neuropathological features of the condition. In TSC, tubers are generally not found in the temporal lobes and tubers in this area are not usually reported as being in the hippocampal formation, which suggests that the deficits were not directly related to the presence of tubers. An explanation could be that the seizure disorder associated with the condition has resulted in a degree of medial temporal lobe sclerosis and grey matter deficits. Although this explanation can only be tested more definitively by further imaging studies of patients with temporal lobe epilepsy uncomplicated by TSC, and/or patients with TSC uncomplicated by epilepsy, we note that the incidence of severe epilepsy in this sample of TSC patients was low (only 3/10 were receiving anticonvulsant medication or had a history of frequent or sustained seizures). The presence of right-sided grey matter deficits in the inferior fronto-parietal lobes was noteworthy because, although tuber distribution over the brain surface is random, tubers tend to proliferate more commonly in the frontal lobes (Scheithauer & Reagan, 1999).

At the level of cognitive performance recent reports of specific deficits in spatial working memory and attentional set-shifting in adults of normal intelligence with TSC (de Vries *et al.* 2001*b*) and of significant sustained attention deficits in children with TSC (de Vries *et al.* 1999) may find neuroanatomical support in this study. Sustained attention networks are known to involve right fronto-parietal systems (Posner & Petersen, 1990) while a recent fMRI study suggests activation of anterior cingulate and bilateral frontal, parietal, temporal and limbic systems during complex investigation tasks such as spatial working memory (Tamminga, 2000).

The white matter deficits in the major intrahemispheric fasciculi are striking and at first sight rather surprising. White matter abnormalities

due to heterotopias and cyst-like changes have been reported, but these are usually considered to be related to a failure in radial migration. However, the cortical tubers that so commonly occur in TSC are likely to be associated with developmental abnormalities in axonal position and hence perhaps abnormalities of the kind reported here. It will be interesting to see if other indices of abnormal connectivity confirm these findings.

Conclusion

We have used contemporary image analysis tools to measure brain structure comprehensively in patients with tuberous sclerosis complex and we have demonstrated extensive and largely symmetrical deficits in limbic and subcortical grey matter and intra-hemispheric white matter tracts. We suggest that these findings may be consistent with the well-known abnormalities in early brain development that determine tuberous sclerosis.

This research was generously supported by a grant to P.F.B from the Tuberous Sclerosis Association. K.R. is supported by the Medical Research Council (UK).

REFERENCE

Ashburner, J. & Friston, K. J. (2000). Voxel-based morphometry: the methods. *NeuroImage* **11**, 805–821

Bolton, P. F. & Griffiths, P. D. (1997). Association of tuberous sclerosis of temporal lobes with autism and atypical autism. *Lancet* **349**, 392–395.

Braffman, B. H., Bilaniuk, L. T., Naidich, T. P., Altman, N. R., Post, M. J. D., Quencer, R. M., Zimmerman, R. A. & Brody, B. A. (1992). MR imaging of tuberous sclerosis – pathogenesis of this phakomatosis, use of gadopentetate dimeglumine, and literature-review. *Radiology* **183**, 227–238.

Brammer, M. J., Bullmore, E. T. & Simmons, A. (1997). Generic brain activation mapping in functional magnetic resonance imaging: a nonparametric approach. *Magnetic Resonance Imaging* **15**, 763–770.

Bullmore, E. T., Brammer, M. J., Rouleau, G., Everitt, B. S., Simmons, A., Sharma, T., Frangou, R., Murray, R. M. & Dunn, G. (1995). Computerised brain tissue classification of magnetic resonance images: a new approach to the problem of partial volume artefact. *NeuroImage* **2**, 133–147.

Bullmore, E. T., Suckling, J., Overmeyer, S., Rabe-Hesketh, S., Taylor, E. & Brammer, M. J. (1999). Global, voxel and cluster tests, by theory and permutation, for a difference between two groups of structural MR images of the brain. *IEEE Transactions on Medical Imaging* **18**, 32–42.

Cox, R. W. (1995). Analysis and visualization of 3D fMRI data. *Proceedings of the 3rd Scientific Meeting of the Society for Magnetic Resonance* **2**, 834.

de Vries, P. J. & Bolton, P. F. (1999). Neuropsychological attentional deficits in children with tuberous sclerosis. *Molecular Psychiatry* **4**, S51.

de Vries, P. J., Hunt, A. & Bolton, P. F. (2001*a*). The psychopathologies of tuberous sclerosis: a study of 510 UK families. *European Child & Adolescent Psychiatry* (submitted).

de Vries, P. J., Harrison, J. E., Sahakian, B., Owen, A. M. & Bolton, P. F. (2001*b*). Specific cognitive deficits in tuberous sclerosis. *Journal of Neurology, Neurosurgery and Psychiatry* (submitted).

Harrison, J. E. & Bolton, P. F. (1997). Annotation: tuberous sclerosis. *Journal of Child Psychology Psychiatry, and Allied Disciplines* **38**, 603–614.

Harrison, J. E., O'Callaghan, F., Hancock, E., Osborne, J. & Bolton, P. F. (1999). Cognitive deficits in normally intelligent patients with tuberous sclerosis. *American Journal of Medical Genetics* (*Neuropsychiatric Genetics*) **88**, 642–646.

Jambaque, I., Cusmai, R., Curatolo, P., Cortesi, F., Perrot, C. & Dulac, O. (1991). Neuropsychological aspects of tuberous sclerosis in relation to epilepsy and MRI findings. *Developmental Medicine and Child Neurology* **33**, 698–705.

Knudson, A. G. (1971). Mutation and cancer: statistical study of retinoblastoma. *Proceedings of the National Academy of Science, USA* **68**, 820–823.

Marti-Bonmati, L., Menor, F. & Dosda, R. (2000). Tuberous sclerosis: differences between cerebral and cerebellar cortical tubers in a pediatric population. *American Journal of Neuroradiology* **21**, 557–560.

Nellist, M., Jansen, B., Carter, P. T. & Hessleingjanssen, A. L. W. (1993). Identification and characterisation of tuberous sclerosis gene on chromosome 16. *Cell* **75**, 1305–1315.

Nelson, H. & Willison, J. (1991). *National Adult Reading Test* (*NART*)*: Test Manual* (*Part II*). NFER-Nelson: Windsor.

Osborne, J. P., Fryer, A. & Webb, D. (1991). Epidemiology of tuberous sclerosis. *Annals of New York Academy of Science* **615**, 125–127.

Posner, M. I. & Petersen, S. E. (1990). The attention system of the human brain. *Annual Review of Neuroscience* **13**, 25–42.

Press, W. H., Teukolsky, S. A., Vetterling, W. T. & Flannery, B. P. (1992). *Numeric Recipes in C: The Art of Scientific Computing* (*2nd ed.*). Cambridge University Press: Cambridge.

Rabe-Hesketh, S., Bullmore, E. T. & Brammer, M. J. (1997). The analysis of functional magnetic resonance images. *Statistical Methods in Medical Research* **6**, 215–237.

Roach, E. S., Gomez, M. R. & Northrup, H. (1998). Tuberous sclerosis complex consensus conference: revised clinical diagnostic criteria. *Journal of Child Neurology* **13**, 624–628.

Scheithauer, B. W. & Reagan, T. J. (1999). Neuropathology. In *Tuberous Sclerosis Complex*, 3rd edn (ed. M. R. Gomez), pp. 101–144. Oxford University Press: Oxford.

Shepherd, C. W., Scheithauer, B. W. & Gomez, M. R. (1991). Subependymal giant cell astrocytoma: a clinical, pathological and flow cytometric study. *Neurology* **28**, 864–868.

Shepherd, C. W., Houser, O. W. & Gomez, M. R. (1995). MR findings in tuberous sclerosis complex and correlation with seizure development and mental impairment. *American Journal of Neuroradiology* **16**, 149–155.

Soucek, T., Pusch, O., Wienecke, R., DeClue, J. E. & Hengstschlager, M. (1997). Role of the tuberous sclerosis gene-2 product in cl1 cycle control. Loss of the tuberous sclerosis gene-2 induces quiescent cells to enter S phase. *Journal of Biological Chemistry* **272**, 29301–29308.

Suckling, J., Sigmundsson, T., Greenwood, K. & Bullmore, E. (1999*a*). A modified fuzzy clustering algorithm for operator independent brain tissue classification of dual echo MR images. *Magnetic Resonance Imaging* **17**, 1065–1076.

Suckling, J., Brammer, M., Lingford-Hughes, A. & Bullmore, E. (1999*b*). Removal of extracerebral tissues in dual-echo magnetic resonance images via linear scale-space features. *Magnetic Resonance Imaging* **17**, 247–256.

Talairach, J. & Tournoux, P. (1988). *Co-planar Stereotaxic Atlas of the Human Brain*. Theme Medical Publishers: New York.

Tamminga, C. A., Shadmehr, R. & Holcomb, H. H. (2000). Images in neuroscience. Cognition: procedural memory. *American Journal of Psychiatry* **157**, 162.

VanSlegtenhorst, M., deHoogt, R., Hermans, C., Nellist, M., Janssen, B., Verhoef, S., Lindhout, D., vandenOuweland, A., Halley, D., Young, J., Burley, M., Jeremiah, S., Woodward, K., Nahmias, J., Fox, M., Ekong, R., Osborne, J., Wolfe, J., Povey, S., Snell, R. G., Cheadle, J. P., Jones, A. C., Tachataki, M., Ravine, D., Sampson, J. R., Reeve, M. P., Richardson, P., Wilmer, F., Munro, C., Hawkins, T. L., Sepp, T., Ali, J. B. M., Ward, S., Green, A. J., Yates, J. R. W., Kwiatkowska, J., Henske, E. P., Short, M. P., Haines, J. H., Jozwiak, S. & Kwiatkowski, D. J. (1997). Identification of the tuberous sclerosis gene TSC1 on chromosome 9q34. *Science* **277**, 805–808.